AIAA JOURNAL
Vol. 46, No. 6, June 2008

# Tip Vortex Control via a Tab Deflecting at Higher Harmonic Frequencies

T. Lee* and J. Pereira†
*McGill University, Montreal, Quebec H3A 2K6, Canada*

DOI: 10.2514/1.29273

**The impact of a trailing-edge tab, actuated at different start times and higher harmonic frequencies, on the size and strength and the position of a tip vortex generated by an oscillating NACA 0015 wing was investigated. The results show that for all the tab control cases tested, the peak tangential velocity of the tip vortex was found to be a weak function of the tab motion, whereas the core radius and circulation were strongly dependent upon the tab deflection. The 2/revolutions higher harmonic tab control actuated during pitch up produced the largest reduction in the peak tangential velocity and the greatest increase in the core radius and also provided the most promising blade-vortex-interaction suppression. Similar control effectiveness was also observed for 3/revolutions higher harmonic tab control motion but to a lesser extent. The 4/revolutions higher harmonic tab control was, however, most effective during the pitch-down flow-reattachment process.**

## Nomenclature

| | | |
|---|---|---|
| $b$ | = | semispan |
| $C_l$ | = | section lift coefficient |
| $C_p$ | = | pressure coefficient |
| $c$ | = | wing chord |
| $d_{\text{miss}}$ | = | vortex-blade miss distance |
| $f_o$ | = | oscillation frequency |
| $L$ | = | lift |
| $l$ | = | span over which 2-D blade-vortex interaction occurs |
| $NP$ | = | nth harmonic of $f_o$ |
| $Re$ | = | Reynolds number, $=u_o c/\nu$ |
| $r$ | = | radial position |
| $r_c$ | = | core radius |
| $t$ | = | time |
| $u$ | = | mean axial velocity |
| $u_o$ | = | freestream velocity |
| $u'$ | = | rms velocity fluctuation |
| $v_\theta$ | = | tangential velocity |
| $x, y, z$ | = | axial, transverse, and span-wise direction |
| $\alpha$ | = | angle of attack |
| $\alpha_m$ | = | mean $\alpha$ |
| $\alpha_{\max}$ | = | maximum $\alpha$ |
| $\alpha_{\min}$ | = | minimum $\alpha$ |
| $\Gamma$ | = | vortex strength or circulation |
| $\Gamma_c$ | = | core circulation |
| $\Gamma_o$ | = | total circulation |
| $\Delta$ | = | BVI parameter, $=\Gamma_c c/(y_c + c)^2 u_o\vert_{\text{controlled}} - \Gamma_c c/(y_c + c)^2 u_o\vert_{\text{uncontrolled}}$ |
| $\delta$ | = | deflection amplitude |
| $\zeta$ | = | streamwise vorticity |
| $\kappa$ | = | reduced frequency, $=\pi f_o c/u_o$ |
| $\nu$ | = | fluid kinematic viscosity |
| $\rho_o$ | = | freestream fluid density |
| $\tau$ | = | phase angle, $=\omega t = 2\pi f_o t$ |

*Subscripts*

| | | |
|---|---|---|
| $d$ | = | pitch down |
| $u$ | = | pitch up |

## I. Introduction

THE impulsive blade-vortex interaction noise, a notable and undesirable characteristic of helicopter low-speed descent flight, is very loud and annoying to the nearby community. This BVI noise is generated by interactions of the rotor blades with the shed concentrated tip vortices from the preceding blades, which induce large unsteady pressure fluctuations on the blade surfaces and, thus, severe dynamic structural loading and impulsive blade-vortex-interaction noise generation. A great deal of progress in the rotor-blade wake measurements and the prediction of blade-vortex-interaction noise generation can be found in the representative work of Mahalingam and Komerath [1], McAlister and Heineck [2], and Duraisamy et al. [3]. Mahalingam and Komerath [1] measured the vortical trailing wake behind a helicopter rotor in forward flight by using LDV and observed that the tip vortex of a rotating blade differed considerably in structure from a fixed-wing vortex. McAlister and Heineck [2] measured the near wake behind a two-bladed model rotor in light climb by using particle image velocimetry (PIV). They reported that the core-radius circulation increased slightly with wake age, but the large-radius circulation appeared to remain relatively constant. The radial distributions of swirl velocity and vorticity exhibited self-similar behaviors, especially within the core. Also, the diameter of the vortex core was initially about 10% of the rotor-blade chord but more than doubled its size after one revolution of the rotor. Duraisamy et al. [3] studied the formation and roll up of a tip vortex trailed from a hovering helicopter rotor blade using both computations and PIV measurements. Secondary and tertiary vortices resulting from cross-flow separations near the blade tip along with a part of the trailed wake, which ultimately entrained into the tip vortex downstream of the trailing edge, were observed.

In addition, it is also known that the rotorcraft BVI noise is a highly complex, three-dimensional, and time-dependent phenomenon. In low-speed descent, there can be multiple BVI events occurring on both the advancing and retreating sides of the rotor disks. Two important blade-vortex interaction extremes occur when the vortex is either normal or parallel to the blade, which are known to have a large influence on rotor aerodynamics, rotor noise, and rotor-blade stress. For the main rotor, the more nearly parallel the tip vortex is to the blade at the time of interaction, the more intense the noise [4–6]. The BVI strength is dominated by two important parameters: the miss distance between the rotor blade and the trailing vortex, and the size (or intensity) of the vortex. Hardin and Lamkin [6] further suggested

Received 12 December 2006; revision received 12 December 2007; accepted for publication 17 February 2008. 

*Associate Professor, Department of Mechanical Engineering.
†Graduate Research Assistant, Department of Mechanical Engineering.

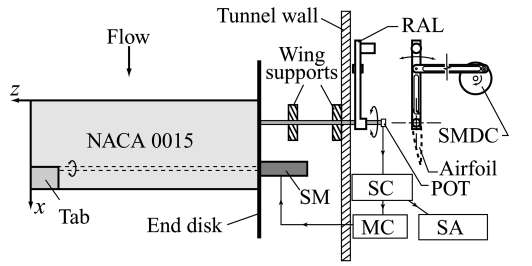


MC: Motor controller
POT: Potentiometer
RAL: Rocker-arm linkage
SA: HP spectrum analyser
SC: Signal conditioner
SM: Servomotor
SMDC: Servomotor-driven crank

a)

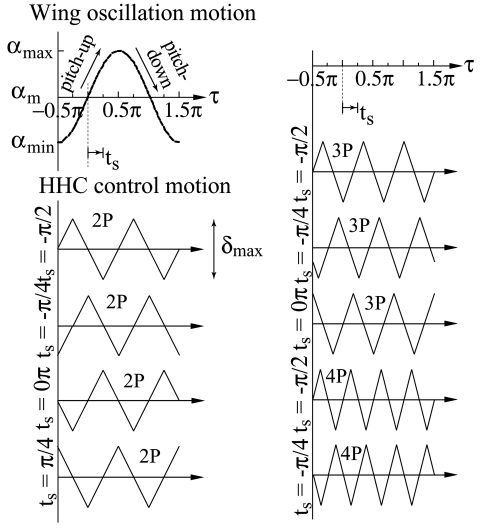


b)

**Fig. 1 a) Experimental setup and b) HHC motion profiles and definitions.**

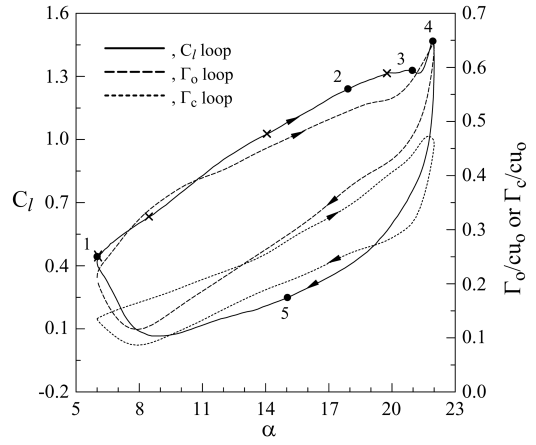


a)

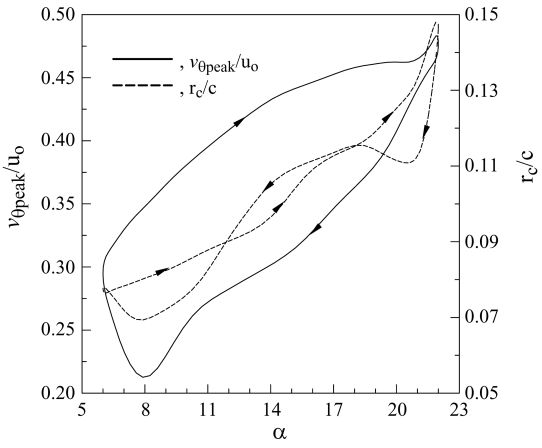


b)

**Fig. 2 Uncontrolled wing. Filled circles denote critical unsteady boundary-layer and dynamic-stall events × symbols denote the start of tab actuation.**

theoretically that the magnitude of the aeroacoustic pressure time history $p(x,t)$ produced by the blade-vortex interactions can be expressed as $p(x,t) \sim \Gamma Ll/\rho_o d_{\text{miss}}^2$. One promising BVI noise reduction concept is therefore to increase the miss distance and/or to decrease the vortex strength and size at the blade-vortex encounters.

A number of passive control devices [7–11] have been attempted to modify the shed vortex structure by altering the blade tip shape, adding other aerodynamic surfaces mounted at the rotor tip (such as winglets, spoiler, stub/subwing, etc.), or blowing air along the vortex axis so as to spread out and diffuse the vortex so that the BVI is weakened and therefore radiates less noise. In the meantime, increasing efforts have also been devoted to implementing active BVI control techniques, which involve a momentary change in blade pitch at just the right azimuth using higher harmonic control (HHC) [12–17], individual blade control [18], and an active trailing-edge tab or flap [19,20]. Among them, the higher harmonic pitch control has been attempted rigorously to obtain reductions in vortex strength and increases in blade-vortex separation distances during vortex-blade encounter so as to reduce the intensity of the BVI fluctuation loading and, thus, noise. Note that although the use of HHC of blade pitch angle has historically been introduced as a means to reduce helicopter vibration levels by implementing active control of the rotor swashplate to change the pitch at the root of the blades, its use to reduce noise offers potential. Past investigations have indicated that higher harmonic pitch control would not only modify pitch but also modify the strength of the shed vortices as well as possibly the interaction locations. The pioneering analytical study in the 1950s by Payne [12] showed the potential effectiveness of HHC in alleviating retreating blade stall. Recently, Enenkl et al. [20] suggested that the way an active trailing-edge servotab reduces noise and vibration may vary depending mainly on flap chord, control frequency, and the blade's torsional stiffness. The details of the vortex flow characteristics, however, were not reported.

The motive of this study was to investigate the possible reduction of the strength and size, and the vertical displacement of the tip vortex, generated behind an oscillating NACA 0015 wing by using a moveable trailing-edge tab operated with 2/rev, 3/rev, and 4/rev (or 2P, 3P, and 4P) HHC pitch inputs at selected phases and amplitudes. The oscillating wing was chosen to simulate the quasiperiodic first harmonic angle-of-attack variations that are found on helicopter

**Table 1 Values of tab motion parameters**

| HHC | $\delta_{\max}$ | $t_s$ | $\alpha_u$ | HHC | $\delta_{\max}$ | $t_s$ | $\alpha_u$ |
|---|---|---|---|---|---|---|---|
| 2P | 16 deg | $-0.5\pi$ | 6 deg $=\alpha_{\min}$ | 3P | 16 deg | $0\pi$ | 14 deg |
| 2P | 16 deg | $-0.25\pi$ | 8.3 deg | 4P | 16 deg | $-0.5\pi$ | 6 deg |
| 2P | 16 deg | $0.0\pi$ | 14 deg $=\alpha_m$ | 4P | 16 deg | $-0.25\pi$ | 8.3 deg |
| 2P | 16 deg | $0.25\pi$ | 19.7 deg | 4P | 16 deg | $0\pi$ | 14 deg |
| 3P | 16 deg | $-0.5\pi$ | 6 deg | 4P | 16 deg | $0.25\pi$ | 19.7 deg |
| 3P | 16 deg | $-0.25\pi$ | 8.3 deg | —— | —— | —— | —— |

rotors during low-speed forward flight [21–23]. Special emphases were placed on the determination of the phase-locked ensemble-averaged core vortex flow parameters, obtained by using a miniature triple hot-wire probe, over one cycle of oscillation. These vortex flow measurements were then used to evaluate the effectiveness of the HHC tab motion on the suppression of BVI noise via the expression suggested by Hardin and Lamkin [6].

## II. Experimental Methods

The experiment was conducted in the 0.9 m × 1.2 m × 2.7 m low-speed suction-type wind tunnel at McGill University with a freestream turbulence intensity of 0.03% at $u_o = 14.2$ m/s. A square-tipped, rectangular, untwisted NACA 0015 airfoil, fabricated from solid aluminum, with $c = 20.3$ cm and $b = 49.5$ cm, was used as the test model. The wing model was mounted horizontally at the center of the wind-tunnel test section. A 40-cm-diam aluminum endplate with sharp leading edges was fixed to an end support located 20 cm from the sidewall of the test section. The origin of the coordinates was located at the wing leading edge. A specially designed four-bar oscillation mechanism, in conjunction with an Exlar model DXM340C servomotor driven by an Emerson model FX3161 PCM1 programmable motion controller, was used to oscillate the wing model through the static-stall angle (=16.5 deg) with $\alpha(t) = 14^\circ + 8^\circ \sin \omega t$ and $\kappa = 0.1$ at $Re = 1.86 \times 10^5$. The oscillation frequency was measured by the use of a potentiometer mounted on the servomotor shaft to an accuracy of ±0.02 Hz. The four-bar mechanism provided an output, which was sinusoidal to within 2%. The airfoil pitch axis was located at the one-fourth-chord location. The instantaneous $\alpha$ of the wing and the phase reference signal were recorded from a potentiometer mounted on the servomotor shaft. Note that when the phase angle was within the range $-0.5\pi \le \tau \le 0.5\pi$, the wing was described to be in pitch up; when $0.5\pi \le \tau \le 1.5\pi$, the wing was said to be in pitch down.

The wing model was equipped with a moveable trailing-edge tab (of a chord of 25%$c$ and a span of 13%$b$), which was activated and

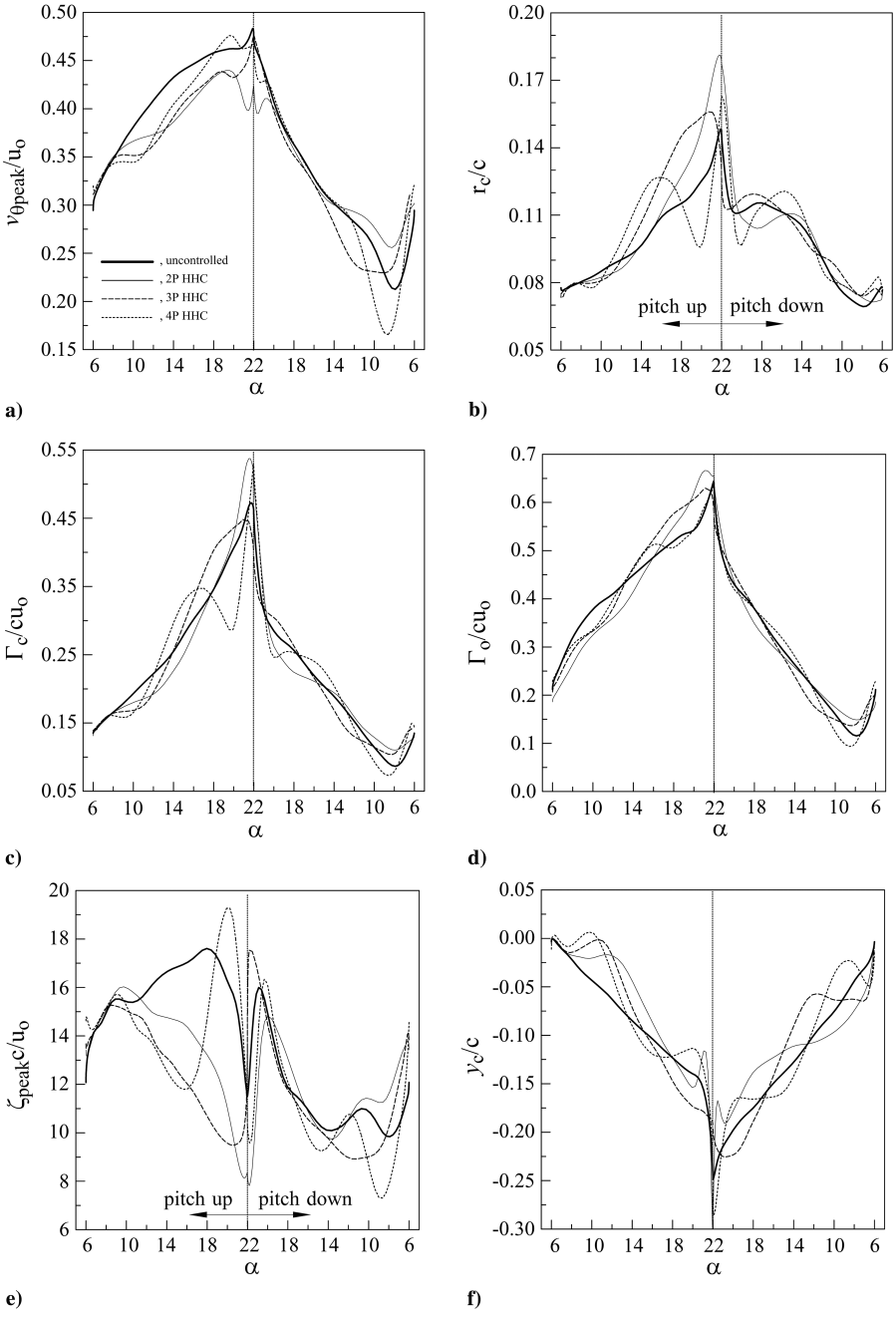


**Fig. 3 Effect of NP on critical vortex flow quantity for $t_s = -0.25\pi$.**

deactivated independently by a Maxon servomotor (model Re-35), incorporating a 4.3:1 helical gearbox and an optical encoder (Fig. 1a). The tab motion, triggered in response to the oscillating wing phase angle $\tau$, can be programmed into a series of saw-tooth deflections. The time of tab actuation (i.e., start time $t_s$) and peak-to-peak deflection amplitude $\delta_{\max}$ (=8 and 16 deg or equivalently $36.4\%\alpha_{\max}$ and $72.8\%\alpha_{\max}$) were determined by a Maxon EPOS 70/10 programmable motion controller. Tab deflections described by an HHC saw-tooth waveform at 2P (i.e., a two-per-oscillation angle-of-attack variation on top of a one-per-oscillation cyclic angle-of-attack), 3P, and 4P of different $t_s$ and $\delta_{\max}$ were employed in the present experiment (Fig. 1b). The tab actuation start time $t_s$ ($= -0.5\pi$, $-0.25\pi$, $0\pi$, and $0.25\pi$, corresponding to $\alpha_u = 6$, 8.3, 14, and 19.7 deg, respectively) were tested to quantify their effects on the critical vortex flow parameters. The parameters describing the tab actuation profile in various units are given in Table 1.

The instantaneous velocities were subsequently ensemble averaged over 40–80 oscillating cycles to obtain phased-locked averages of the vortex flow properties at various phase positions during the cycle. A miniature triple hot-wire probe (Auspex Model AVEP-3-102 with a measurement volume of 0.5 $mm^3$) was used to measure the mean and fluctuating velocity components in planes perpendicular to the freestream velocity at $x/c = 3.0$. The triple-hot-wire probe was calibrated in situ, following the calibration procedures described by Chow et al. [24], before the installation of the model. The hot-wire signals were sampled at 500 Hz and were recorded on a PC through a 16-bit A/D converter board. Probe traversing was achieved through a custom-built computer-controlled traversing system. Data plane taken in the near field of the wing model had $56 \times 56$ measuring grid points with an increment of $\Delta y = \Delta z = 1.6$ mm (or $0.8\%c$). The streamwise vorticity was calculated by differentiation according to $\zeta = \partial w/\partial y - \partial v/\partial z$. The maximum experimental uncertainties in the results reported have been estimated as follows: mean velocity 3.5%, vorticity component 8%, vortex radius 4%, and velocity fluctuation 3%.

## III. Results and Discussion

### A. Uncontrolled Wing

To better understand the impact of the HHC tab motion on the tip-vortex flow characteristics (such as the peak tangential velocity $v_{\theta\text{peak}}$, core radius $r_c$, core $\Gamma_c$, total $\Gamma_o$ circulation, and the vortex position), the variation of $v_{\theta\text{peak}}$, $r_c$, $\Gamma_c$, and $\Gamma_o$ of the baseline, or uncontrolled, wing with $\alpha$ over an oscillation cycle is discussed first in Fig. 2 and also serves as a comparison. Also presented in Fig. 2a is the dynamic $C_l$–$\alpha$ loop, calculated via the $C_p$ distributions obtained from 48 0.35-mm-diam pressure taps distributed over the upper and lower surfaces of the wing model [25], of the 2-D wing. Figure 2a shows that for a NACA 0015 wing oscillated with $\alpha(t) = 14 \text{ deg} + 8 \text{ deg} \sin \omega t$ and $\kappa = 0.1$, the unsteady boundary layer remained attached up to $\alpha_u \approx 18$ deg (denoted by point 2) and was followed by the onset of flow reversal and its upstream propagation for $\alpha_u \approx 18$ to 21 deg (denoted by points 2 to 3). With a further increase in $\alpha$ (from $\alpha_u \approx 21$ deg to $\alpha_{\max} = 22$ deg; points 3 to 4), there was a brief presence of a dynamic-stall vortex (DSV) of about $30\%c$ observed in the leading-edge region of the upper wing surface [26]. The DSV was "spilled" prematurely (a characteristic of a light-stall oscillation [21,22]) as soon as the pitch-down process began, resulting in a drastic during-stall $C_l$ loss, and was followed by a gradual $C_l$ recovery for $\alpha_d \approx 15$ to 6 deg (denoted by points 5 to 1) during the pitch-down flow-reattachment flow process.

Figure 2a also indicates that, as expected, a similar variation in the total circulation $\Gamma_o$ (indicative of the bound circulation and thus the $C_l$ value), corresponding to the $C_l$-$\alpha$ variation over an oscillation cycle, was also noticed. The circulation, or vortex strength, was obtained by summing the vorticity multiplied with the incremental area of the measuring grid. The value of $\Gamma_o$ generally followed the change in $C_l$ data (up to $\alpha_u \approx 18$ deg) during pitch-up attached-flow process, whereas an increasing discrepancy appeared for 18 deg $< \alpha_u <$ 21 deg due to the presence of flow reversal. Note that the $\Gamma_o$ had a noticeably smaller value during pitch down than during pitch up. A core circulation-to-total circulation $\Gamma_c/\Gamma_o$ ratio ranging between 0.5 and 0.76, coinciding with the attached-flow and DSV-formation-flow processes, respectively, was observed. The peak tangential velocity was also found be of higher value during pitch up than during pitch down (Fig. 2b), suggesting that during pitch down, the vortex had a much smaller rotational speed compared with the vortex during pitch up. In contrast to the large variation observed in $v_{\theta\text{peak}}$ and $\Gamma_c$ during pitch up and pitch down, the value of the core radius $r_c$ (identified by the location of $v_{\theta\text{peak}}$) was found to be generally small, within measurement error, regardless of pitch-up or pitch-down flow process, except during DSV spillage. In summary, a maximum (minimum) $C_l$, $\Gamma_o/cu_o$, $\Gamma_c/cu_o$, $v_{\theta\text{peak}}/u_o$, and $r_c/c$ of 1.45, 0.65, 0.475, 0.49, and 0.148 at $\alpha_{\max}$, and a minimum 0.08, 0.11, 0.09, 0.21, and 0.07 at $\alpha_d \approx 8$ deg were observed, respectively. Note also that because of the convection time required for a tip-vortex flow structure to propagate from the wing to the downstream location of the sensor, there is a phase lag between any instantaneous sensor reading and the position of the wing at that instantaneous instant. By assuming that, within the streamwise length scale considered, any streamwise distortion of the flow that occurs is negligible, and the convection speed $u_{\text{conv}}$ is constant, then the angle of attack through which the wing has swept during the convection time can be directly calculated if $u_{\text{conv}}$ can then be approximated. An upper and lower bound is subsequently imposed upon the convection

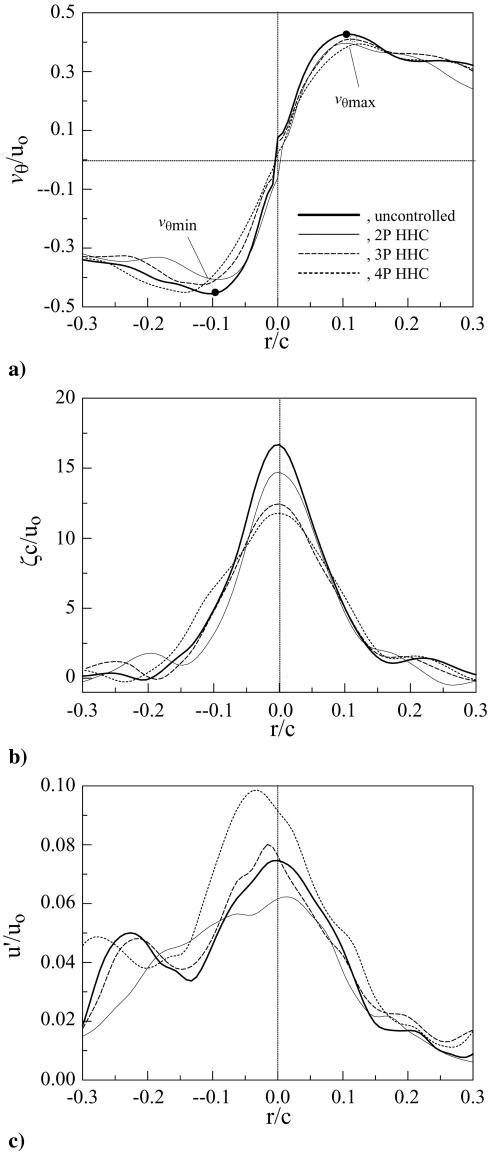


**Fig. 4 Typical vortex flow distribution across vortex center along *y* axis for $\alpha_u = 15$ deg and $t_s = -0.25\pi$.**

speed because it cannot fall outside of the range of axial velocities measured within the volume through which it has moved. In the present experiment, $u_{\text{conv}}$ was approximated as the upper-bound freestream speed because it resulted in the smallest phase-lag correction and, by extension, a more conservative result. The compensation scheme proposed by Chang and Park [27], in which $u_{\text{conv}}$ was approximated with a spatial average axial velocity in the vicinity of the vortex core, could somewhat inflate the convection speed. The measurements reported in this study were phase-lag compensated by letting $u_{\text{conv}} = u_o$.

### B. Effects of NP

The influence of higher harmonic tab motion (i.e., $NP = 2$P, 3P, and 4P), actuated at $t_s = -0.25\pi$ (or $\alpha_u = 8.3$ deg during pitch up) with $\delta_{\max} = 16°$, on the magnitude of $v_{\theta\text{peak}}$, $r_c$, $\Gamma_c$, $\Gamma_o$, the peak vorticity $\zeta_{\text{peak}}$, and the vertical position of the vortex center $y_c$ is summarized in Fig. 3. For clarity, the dynamic variation of these parameters over an entire oscillation cycle is presented in an unfolded format in contrast to the closed-loops presented in Fig. 2. The overall change in $v_{\theta\text{peak}}$, $r_c$, and $\Gamma_c$ with NP, compared with the uncontrolled wing, can be clearly seen (Figs. 3a–3c). These changes were found to be quite substantial starting from $\alpha_{\min}$ up to the moment of DSV spillage, although they were of much lesser extent during poststall because the tab deflection was embedded in the DSV-induced separated flow region. A substantial suppression of $v_{\theta\text{peak}}$ was, however, reestablished during the pitch-down flow-reattachment flow process. Also, similar to the uncontrolled wing, the hysteretic property existing in $v_{\theta\text{peak}}$, $r_c$, $\Gamma_c$, and $\Gamma_o$ (Fig. 3d) between pitch up and pitch down was also exhibited, regardless of NP. The present measurements also reveal that for all the HHC tab control tested with $\delta = \pm 4$ deg, the variation of the critical vortex flow parameters followed those of $\delta = \pm 8$ deg (or $\delta_{\max} = 16$ deg) but had a much lesser extent, and is, therefore, not reported here.

Figure 3a further shows that for a 2P tab motion actuated at $t_s = -0.25\pi$, the peak tangential velocity was always reduced during pitch up and DSV spillage. The observed reduction in $v_{\theta\text{peak}}$ was accompanied by a more diffused vortex with an increased $r_c$ (Fig. 3b). However, in contrast to the smallest $v_{\theta\text{peak}}$ observed at around $\alpha_{\max}$ (as much as 23% below that of the uncontrolled wing), the 2P tab control case rendered a highest $v_{\theta\text{peak}}$ value (above the uncontrolled wing) during pitch-down flow reattachment among the three NP tested. There was no significant variation in $v_{\theta\text{peak}}$, regardless of NP, during stall. The consecutive upward and downward 2P tab deflections also led to a decreased $\Gamma_c$ during pitch up for $\alpha_u \leq 18$ deg and an increased $\Gamma_c$ for $\alpha_u = 18$ deg to $\alpha_d = 21$ deg (Fig. 3c). A maximum 13% increase in $\Gamma_c$ at $\alpha \approx \alpha_{\max}$ was observed for the 2P control case. The results also show that a similar variation (but of a much lesser extent) in $\Gamma_o$ with NP, compared with $\Gamma_c$, was also observed (Fig. 3d). It can therefore be concluded that although very effective at controlling the vortex core flow quantity, regardless of NP, the HHC tab motion did not exercise significant control on the vortex in its entirety. Figures 3a–3c further reveal that the 3P tab control also provided a reduction in $v_{\theta\text{peak}}$ but was accompanied by more a drastic deviation in $r_c$ and $\Gamma_c$ during pitch up in comparison to the 2P control case. Special attention should be given to the drastic reduction in $r_c$ and $\Gamma_c$ (i.e., a more concentrated vortex core of a reduced circulation) for $\alpha_u = 18$ to 21.5 deg for the 4P HHC control case.

Figure 3e reveals that the 2P and 3P control cases always rendered a substantial decrease (as much as 40% below the uncontrolled wing) in the peak vorticity $\zeta_{\text{peak}}$ during the pitch-up and during-stall flow

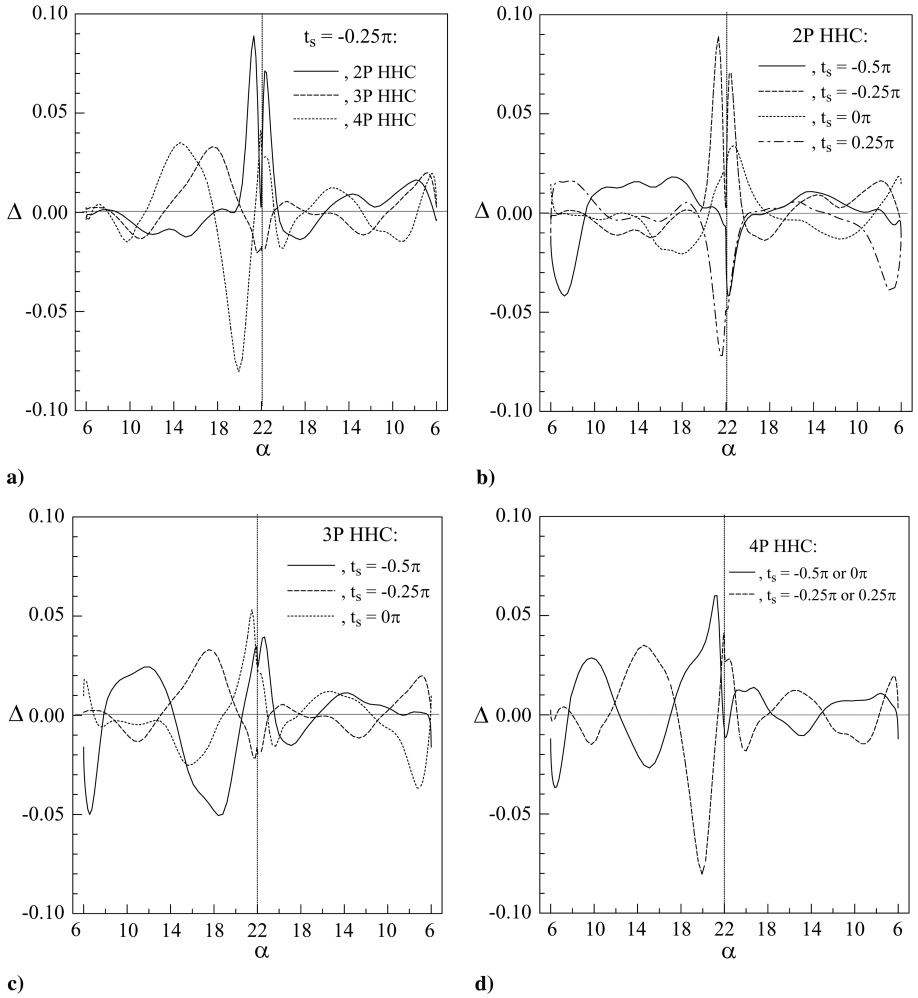


**Fig. 5 Variation of Δ with NP and $t_s$.**

processes. For 4P tab control, $\zeta_{peak}$ was, however, found to decrease first, reaching a local minimum at $\alpha_u = 16$ deg and was followed by a consistent increase with increasing $\alpha$ until $\alpha_u = 20$ deg. The variation in $\zeta_{peak}$ during pitch down was also found to be of much less degree compared with during pitch up, regardless of NP. The impact of the HHC tab motion on the vortex core flow can also be reflected from the distributions of $v_\theta$ and $\zeta$ across the vortex center (identified by the location of $\zeta_{peak}$) along the $y$ axis, for example, at $\alpha_u = 15$ deg, displayed in Figs. 4a and 4b. The variation of $v_{\theta peak}$ and $\zeta_{peak}$ with NP can be clearly seen. Note that for a nearly axisymmetric vortex the $v_\theta$ and $\zeta$ distributions (for $\alpha_u < 17$ deg) are independent of the azimuthal angle and had $|v_{\theta\max}| \approx |v_{\theta\min}|$. For $\alpha_u > 17$ deg, the vortex shape was distorted and the core vortex flow values reported are circumferentially averaged values. The present measurements also show that the 2P control case generally produced a lowered $u'$ compared with that of the uncontrolled wing (Fig. 4c), whereas the 3P and 4P control cases rendered an elevated level of streamwise velocity fluctuations. Note the pronounced and consistent increase in $u'$ as the vortex center was approached, regardless of NP, suggesting that the vortex center could be of turbulent nature. No vortex meandering compensation was employed in the data presented in Fig. 4c. However, it is known that in the near field, the *rms* amplitude of the meandering is generally less than $0.5\%c$ which led to a maximum 5 and 6% vortex-meandering-induced variation in the core radius and the peak tangential velocity [28], respectively, and that the effects of vortex meandering only gains significance in the far field [23]. Additional measurements are needed to quantify the vortex meandering associated with the unsteady-wing experiments.

The present measurements also show that, in addition to the observed significant impact of the HHC tab motion on $v_{\theta peak}$, $r_c$, and $\Gamma_c$, a large vertical displacement of the vortex center, that is, $y_c$ throughout the entire oscillation cycle, was also achieved (Fig. 3f). It is of importance to note that the present $\Gamma_c$ and $y_c$ measurements also provide a comparative assessment of the potential HHC tab control of the BVIs via Hardin and Lamkin's prediction. An estimator $\Delta$

$$= \Gamma_c c/(y_c + c)^2 u_o|_{\text{controlled}} - \Gamma_c c/(y_c + c)^2 u_o|_{\text{uncontrolled}}$$

which is equal to the difference between the magnitude of $\Gamma/d_{\text{miss}}^2$ between a tip vortex with and without a tab, was used to evaluate the potential of the HHC tab control of the BVI strength. Figure 5a shows that the 2P control case provided a relative better improvement in $\Delta$ ($<0$) during pitch up compared with the 3P and 4P control cases, except in the vicinity of $\alpha_{\max}$. The 4P control was found to provide the most significant BVI suppression at $\alpha \approx \alpha_{\max}$. No significant discrepancy in $\Delta$ was, however, noticed during pitch down for the three NP tested.

### C. Effects of $t_s$

The variation of the magnitude of the phase-locked ensemble-averaged $\zeta_{peak}$, $r_c$, $\Gamma_c$, $v_{\theta peak}$, $y_c$, and $\Delta$ with the tab actuation start time $t_s$ ($= -0.5\pi, -0.25\pi, 0\pi$, and $+0.25\pi$) is presented in Figs. 5–8. For 2P tab control, the $t_s = -0.5\pi$ and $-0.25\pi$ control cases led to a considerably reduced $\zeta_{peak}$ during pitch up (Fig. 6a); the earlier the

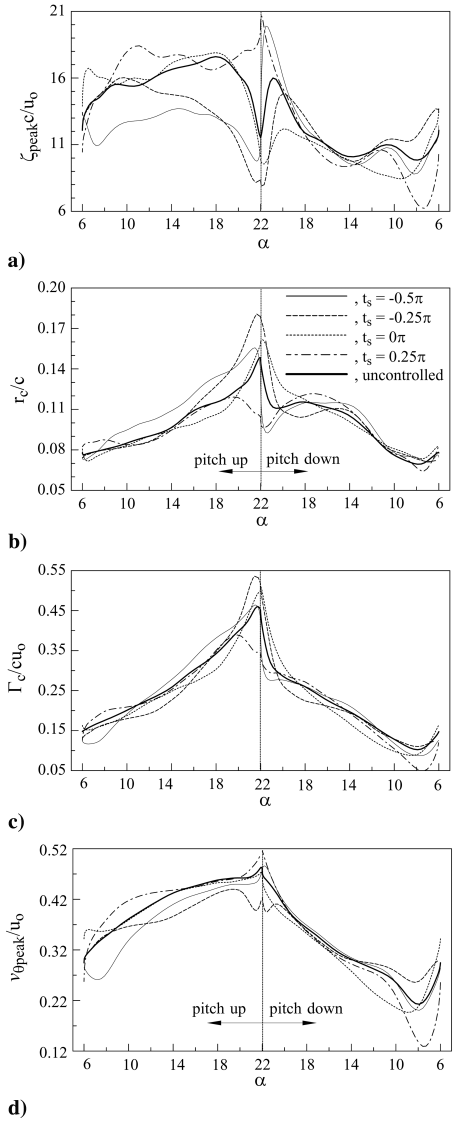


**Fig. 6 Variation of critical vortex flow quantity with $t_s$ for 2P HHC.**

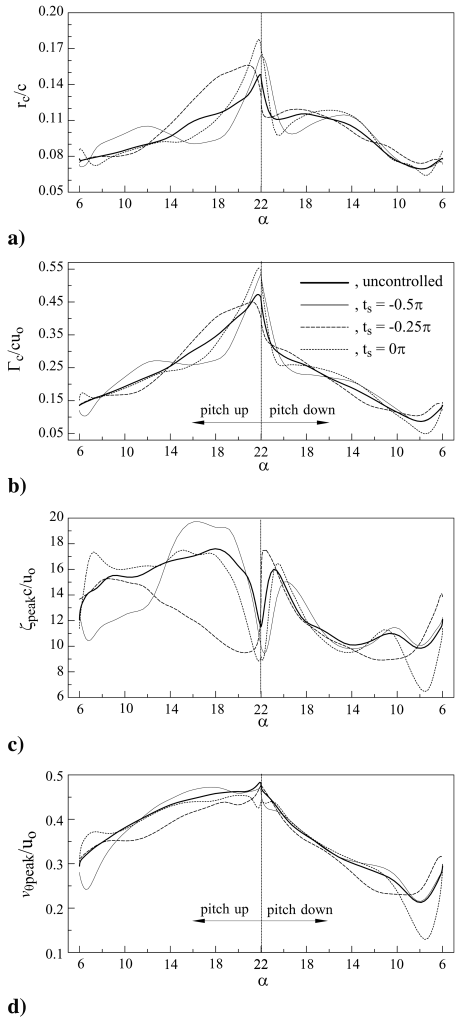


**Fig. 7 Variation of critical vortex flow quantity with $t_s$ for 3P HHC.**

tab actuation, the smaller, in general, $\zeta_{peak}$ was. The $t_s = 0\pi$ and $+0.25\pi$ control cases, however, created a rather minor change in $\zeta_{peak}$. The 2P control case with $t_s = -0.5\pi$ was found to be most effective in the reduction of $\zeta_{peak}$, and, subsequently, a more diffused vortex of enlarged $r_c$ (Fig. 6b) with a slightly increased $\Gamma_c$ (Fig. 6c). During pitch-down flow reattachment, the later the tab actuation, the lower the $\zeta_{peak}$ became (except the $t_s = -0.25\pi$ control case), whereas the values of $r_c$ and $\Gamma_c$ remained virtually unchanged. Furthermore, the $v_{\theta peak}$ was found to be reduced for $t_s < 0\pi$, while equal to or slightly above the uncontrolled wing for $t_s \geq 0\pi$. Note that the $t_s = -0.25\pi$ control case provided the lowest $v_{\theta peak}$ among the $t_s$ tested, except for the pitch-down flow-reattachment flow regime and early on in the upstroke. A local peak in $r_c$ and $\Gamma_c$ and a local minimum in $\zeta_{peak}$ at $\alpha_{max}$ was also observed for the $t_s = -0.25\pi$ control case. Figures 6a–6d also reveal that the hysteresis associated with $\zeta_{peak}$, $r_c$, $\Gamma_c$, and $v_{\theta peak}$ was also found to be generally narrowed with earlier tab actuation. The vertical displacement of the vortex center, implying the potential collision of the blade leading edge with the vortex, was evaluated together with the variation in $\Gamma_c$ in terms of $\Delta$ (Fig. 5b). Figure 5b indicates that, in general, the later the tab actuation, the more effective the BVI suppression during pitch up. The $t_s = 0.25\pi$ control case provided the largest local reduction in $\Delta$ at around $\alpha_{max}$, whereas the $t_s = -0.25\pi$ control case provided the most unfavorable BVI suppression.

For 3P tab control, the change in $r_c$ (Fig. 7a) was accompanied by a corresponding increase and decrease in $\Gamma_c$ (Fig. 7b) and $\zeta_{peak}$ (Fig. 7c), respectively. An opposite change in magnitude of $v_{\theta peak}$ (Fig. 7d) in comparison to the variation observed for $r_c$ was noticed. The $t_s = -0.25\pi$ control case led to a generally more diffused vortex (for $\alpha_u = 14$ to 21 deg) and a significantly reduced $v_{\theta peak}$ and $\zeta_{peak}$ compared with the uncontrolled wing during pitch up. The $t_s = 0\pi$ control provided the lowest $v_{\theta peak}$ and $\Gamma_c$ during the final stage of the pitch-down flow-reattachment flow process. The $\Delta$ calculation, however, shows that the $t_s = -0.25\pi$ control case created a maximum BVI alleviation at $\alpha_{max}$, whereas the $t_s = 0\pi$ control case seemed to be a more effective, except in the vicinity of $\alpha_{max}$ in terms of $\Delta$ (Fig. 5c). The present measurements also indicate that for 4P tab control actuated at different $t_s$, the $t_s = -0.25\pi$ and $0.25\pi$ control cases provided a relatively improved $\Delta$ parameter compared with the $t_s = -0.5\pi$ and $0\pi$ control cases (Fig. 5d).

A more in-depth look into the response of $v_{\theta peak}$, $r_c$, $\Gamma_c$, and $y_c$ can be revealed by looking at the increment relative to the uncontrolled

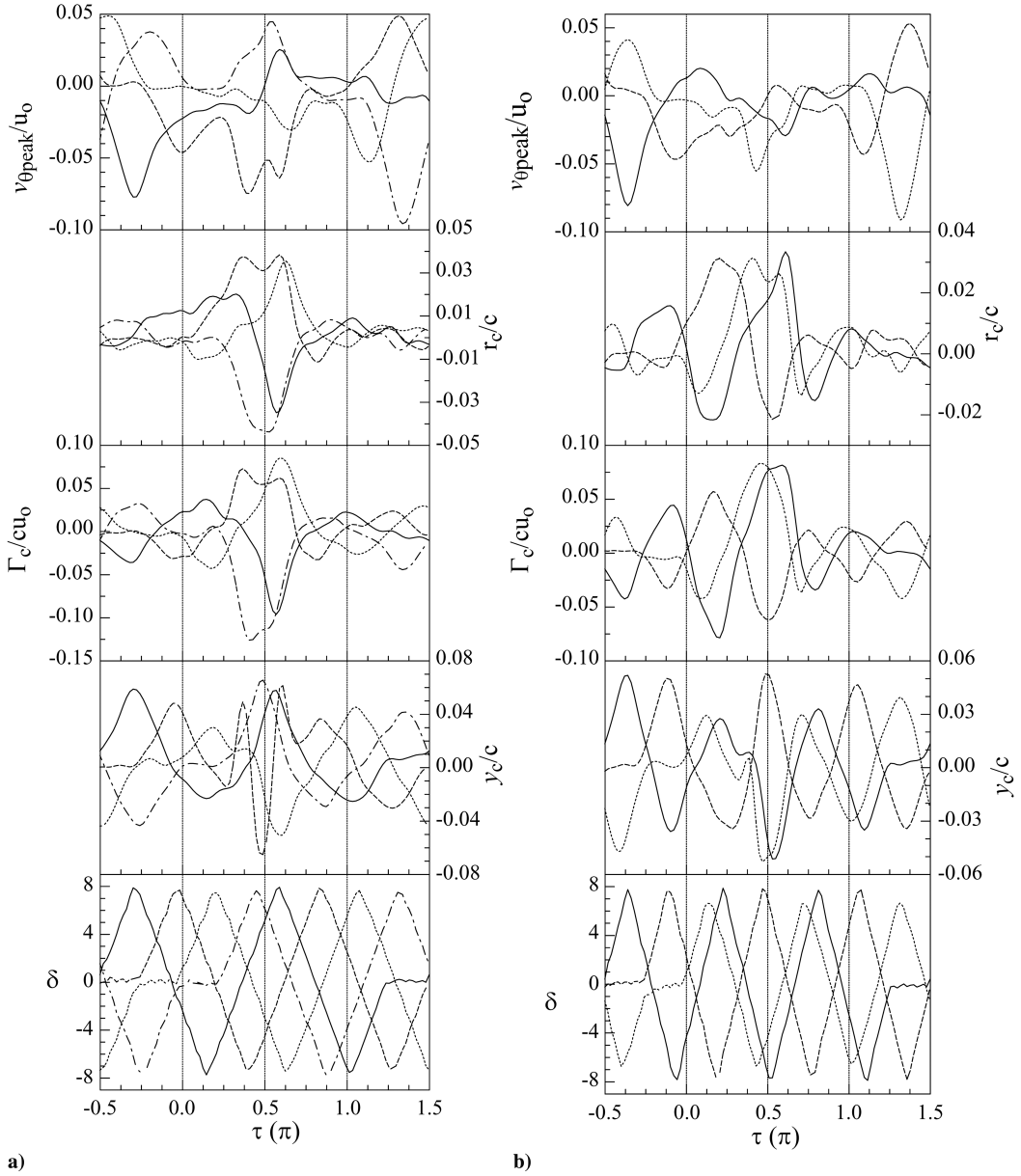


**Fig. 8 Vortex flow quantities relative to uncontrolled wing. a) 2P and b) 3P. Solid line, $t_s = -0.5\pi$; dashed line, $t_s = -0.25\pi$; dotted line, $t_s = 0\pi$; dashed-dotted line, $t_s = +0.25\pi$.**

wing as a function of phase angle. Note that in the following discussion, the variation of these tip-vortex quantities is described as inversely proportional, or inverse, when it decreases with increasing tab angle $\delta$ and increases with decreasing $\delta$, and directly proportional, or proportional, when it increases with increasing $\delta$ and decreases with decreasing $\delta$. For the 2P control cases (Fig. 8a), $v_{\theta\text{peak}}$ varied inversely with tab motion except in the period between the formation of the DSV (at $\alpha_u \approx 20$ deg) and the beginning of flow reattachment (at $\alpha_d \approx 16$ deg) when it varied proportionally, irrespective of $t_s$. The tab had no noticeable effect on $v_{\theta\text{peak}}$ when the flow was completely separated. The $r_c$ also varied inversely with the tab motion, however, with two exceptions; 1) for $t_s = -0.5\pi$, the response of $r_c$ during the attached-flow phase was to make the vortex more diffused regardless of the tab motion being up or down, and 2) for $t_s = -0.25\pi$, before $\alpha_u \approx 14$ deg and subsequent to $\alpha_d \approx 12$ deg, $r_c$ did not change significantly. Interestingly, of all the parameters, it was $\Gamma_c$ that followed most closely the tab motion, albeit with an inverse relation. With regards to $\zeta_{\text{peak}}$, the oscillation cycle was divided into two distinct portions. In one portion, the $\zeta_{\text{peak}}$ variation was inversely proportional to $\delta$, whereas in the other portion it was directly proportional. In general, the $\zeta_{\text{peak}}$ variation began the cycle inversely proportional, switched to directly proportional during pitch up (the time of the switch increased with $t_s$), and then changed back to inversely proportional (usually near $\alpha_d \approx 13$ deg). Lastly, as expected, the location of the vortex center $y_c$ followed quite closely the motion of the tab. An upwards or downwards deflection induced an upwards or downwards displacement, respectively. Note, however, that $y_c$ oscillated somewhat during the DSV formation and spillage, being rather significant for the $t_s = -0.25\pi$ and $t_s = 0\pi$ control cases.

For the 3P control case (Fig. 8b), similar statements can be made as for the 2P control case. The $v_{\theta\text{peak}}$, in general, followed the tab motion quite closely; however, there existed sometimes a short delay when the tab changed direction. The relation to $\delta$ was similar to that of $\zeta_{\text{peak}}$ in the 2P case (i.e., it changed from inverse, to direct, and then back to inverse). The value of $r_c$ varied inversely with $\delta$. The value of $\Gamma_c$ follows extremely faithfully the tab motion. This is most predominant for $t_s = -0.5\pi$ and $t_s = 0\pi$ and is rather minor for $t_s = -0.25\pi$. Conversely, the $\zeta_{\text{peak}}$ was, in general, found not to respond in any predictable way to the tab motion. There are certain instances in which $\zeta_{\text{peak}}$ followed, either inversely or proportionally, the tab motion; these instances, however, were interspersed in an otherwise irregular trend. Contrary to $\zeta_{\text{peak}}$, the vortex center tracked very closely the motion of the tab. For the 4P control case (not shown here), the magnitude of $v_{\theta\text{peak}}$ and $\zeta_{\text{peak}}$ suggests that the tab motion exceeded the response time of the tip vortex because no general trend was discernible; sometimes they followed the tab motion inversely, sometimes proportionally, and sometimes not at all. Furthermore, there seemed to be a phase lag. On the contrary, $r_c$, $\Gamma_c$, and $y_c$ did track the tab motion quite well. The value of $y_c$ was directly proportional to, and followed closely, the tab motion, except during the DSV formation, where it deviated slightly.

## IV. Conclusions

The impact of prescheduled higher harmonic tab motion on the characteristic tip-vortex flow structure, generated behind an oscillating NACA 0015 wing, was investigated at $Re = 1.86 \times 10^5$. These vortex flow measurements were then used to estimate the effectiveness of potential BVI suppression. For all the tab control motions tested, the peak tangential velocity was observed to be a weak function of the tab motion, whereas the core radius and circulation and the peak vorticity were strongly dependent upon the tab motion. The 2P tab control produced the largest reduction in the peak tangential velocity and vorticity and the largest increase in the core radius and circulation, as well as the maximum BVI suppression. The 3P HHC tab control provided a similar variation in the core vortex flow quantities but to a lesser extent compared with 2P tab control. The 4P tab control created a strong control of the vortex flow during pitch-down flow reattachment. In summary, the higher harmonic tab control of the unsteady-wing tip vortex and the subsequent BVI strength seems favorable; experiments with a rotating wing model, however, are needed to further support the findings reported here.

## Acknowledgments

This work was supported by the Natural Science and Engineering Research Council (NSERC) of Canada. P. Gerontakos is thanked for his rigorous help with the experiment.

## References

[1] Mahalingam, R., and Komerath, N. M., "Measurements of the Near-Wake of a Helicopter Rotor in Forward Flight," AIAA Paper 98-0692, 1998.

[2] McAlister, K. W., and Heineck, J. T., "Measurement of the Early Development of Trailing Vorticity from a Rotor," NASA TP-2002-211848, 2002.

[3] Duraisamy, K., Ramasamy, M., and Leishman, J. G., "Computational/Experimental Study of Hover Rotor Tip Vortex Formation," *62nd Annual National Forum of American Helicopter Society*, 2006, pp. 1–18.

[4] Schmtiz, F. H., and Sim, B. W., "Radiation and Directionality Characteristics of Helicopter Blade-Vortex Interaction Noise," *Journal of the American Helicopter Society*, Vol. 48, No. 4, 2003, pp. 253–269.

[5] Brentner, K. S., and Farassat, F., "Modeling Aerodynamically Generated Sound of Helicopter Noise," *Progress in Aerospace Sciences*, Vol. 39, Nos. 2–3, 2003, pp. 83–120. doi:10.1016/S0376-0421(02)00068-4

[6] Hardin, J. C., and Lamkin, S. L., "Concepts for Reduction of Blade/Vortex Interaction Noise," *Journal of Aircraft*, Vol. 24, No. 2, 1987, pp. 120–125.

[7] Tangler, J. L., "Experimental Investigation of the Subwing Tip and Its Vortex Structure," NASA CR-3058, 1978.

[8] Muller, R. H. G., "Winglets on Rotor Blades in Forward Flight: A Theoretical and Experimental Investigation," *Vertica*, Vol. 14, No. 1, 1990, pp. 31–46.

[9] Liu, Z., Russell, J. W., Sankar, L. N., and Hassan, A. A., "A Study of Rotor Tip Vortex Structure Alternation Techniques," *Journal of Aircraft*, Vol. 38, No. 3, 2001, pp. 473–477.

[10] McAlister, K. W., Tung, C., and Heineck, J. T., "Devices That Alter Tip Vortex of a Rotor," NASA TM-2001-209625, 2001.

[11] Han, Y. O., and Leishman, J. G., "Investigation of Helicopter Rotor-Blade-Tip-Vortex Alleviation Using a Slotted Tip," *AIAA Journal*, Vol. 42, No. 3, 2004, pp. 524–535. doi:10.2514/1.3254

[12] Payne, P. R., "Higher Harmonic Rotor Control," *Aircraft Engineering*, Vol. 30, No. 354, 1958, pp. 222–226. doi:10.1108/eb033045

[13] Wood, E. R., Powers, R. W., Hammond, C. E., and Cline, J. H., "On Developing and Flight Testing a Higher Harmonic Control System," *Journal of the American Helicopter Society*, Vol. 30, No. 1, 1985, pp. 3–20.

[14] Shaw, J., Albion, N., Hanker, E. J., and Teal, R. S., "Higher Harmonic Control: Wind Tunnel Demonstration of Fully Effective Vibratory Hub Force Suppression," *Journal of the American Helicopter Society*, Vol. 34, No. 1, 1989, pp. 14–25.

[15] Brooks, T. F., Booth, E. R., Jolly, J. R., Yeager, W. T., and Wilbur, M. L., "Reduction of Blade-Vortex Interaction Noise Through Higher Harmonic Pitch Control," *Journal of the American Helicopter Society*, Vol. 35, No. 1, 1990, pp. 86–91.

[16] Splettstoesser, W. F., Schultz, K. J., Kube, R., Brooks, T. F., Booth, E. R., Niesl, G., and Streby, O., "A Higher Harmonic Control Test in the DNW to Reduce Impulsive BVI Noise," *Journal of the American Helicopter Society*, Vol. 39, No. 4, 1994, pp. 3–13.

[17] Cheng, R. P., Theodore, C. R., and Celi, R., "Effects of 2/rev Higher Harmonic Control on Rotor Performance," *56th Annual Forum of the American Helicopter Society*, May 2000, pp. 1–35.

[18] Yong, C., Zimcik, D. G., Wickramasinghe, V. K., and Nitzsche, F., "Development of the Smart Spring for Active Vibration Control of Helicopter Blades," *Journal of Intelligent Material Systems and Structures*, Vol. 15, No. 1, 2004, pp. 37–47.

[19] Straub, F. K., Ngo, H. T., Anand, V., and Domzalski, D., "Development of a Piezoelectric Actuator for Trailing-Edge Flap Control of Full Scale Rotor Blades," *Smart Materials and Structures*, Vol. 10, No. 1, 2001, pp. 25–34. doi:10.1088/0964-1726/10/1/303

[20] Enenkl, B., Kloppel, V., Preibler, D., and Janker, P., "Full Scale Rotor with Piezoelectric Actuated Blade Flaps," *28th Europe Rotorcraft Forum*, 17–19 Sept. 2002.
[21] McAlister, K. W., Carr, L. W., and McCroskey, W. J., "Dynamic Stall Experiments on the NACA 0012 Airfoil," NASA TP-1100, 1978.
[22] McCroskey, W. J., "Unsteady Airfoils," *Annual Review of Fluid Mechanics*, Vol. 14, 1982, pp. 285–311. doi:10.1146/annurev.fl.14.010182.001441
[23] Ramaprian, B. R., and Zheng, Y., "Near Field of the Tip Vortex Behind an Oscillating Rectangular Wing," *AIAA Journal*, Vol. 36, No. 7, 1998, pp. 1263–1269.
[24] Chow, J. S., Zilliac, G. G., and Bradshaw, P., "Mean and Turbulence Measurements in the Near Field of a Wingtip Vortex," *AIAA Journal*, Vol. 35, No. 10, 1997, pp. 1561–1567.
[25] Gerontakos, P., and Lee, T., "Dynamic-Stall Flow Control via a Trailing-Edge Flap," *AIAA Journal*, Vol. 44, No. 3, 2006, pp. 469–480.
[26] Lee, T., and Gerontakos, P., "Investigation of Flow over an Oscillating Airfoil," *Journal of Fluid Mechanics*, Vol. 512, 2004, pp. 313–341.
[27] Chang, J. W., and Park, S. O., "Measurement in the Tip Vortex Roll-Up Region of an Oscillating Wing," *AIAA Journal*, Vol. 38, No. 6, 2000, pp. 1092–1095.
[28] Devenport, W. J., Rife, M. C., Liapis, S. I., and Follin, G. J., "The Structure and Development of a Wing-Tip Vortex," *Journal of Fluid Mechanics*, Vol. 312, 1996, pp. 67–106. doi:10.1017/S0022112096001929

E. Gutmark
*Associate Editor*